Chinese Chemical Letters 35 (2024) 109455

Contents lists available at ScienceDirect

Chinese Chemical Letters

journal homepage: www.elsevier.com/locate/cclet

Single-atom Pd anchored in the porphyrin-center of ultrathin 2D-MOFs as the active center to enhance photocatalytic hydrogen-evolution and NO-removal

Xingyan Liu[a,1], Chaogang Jia[a,1], Guangmei Jiang[a], Chenghua Zhang[b,*], Mingzuo Chen[a], Xiaofei Zhao[c,*], Xiaocheng Zhang[a], Min Fu[a], Siqi Li[d], Jie Wu[e], Yiming Jia[f], Youzhou He[a,*]

[a] *Chongqing Key Laboratory of Catalysis and New Environmental Materials, College of Environment and Resources, Chongqing Technology and Business University, Chongqing 400067, China*
[b] *School of Pharmacy, North Sichuan Medical College, Nanchong 637100, China*
[c] *Carbon Neutrality Technology Application Research Center, College of River and Ocean Engineering, Chongqing Jiaotong University, Chongqing 400074, China*
[d] *State Key Joint Laboratory of Environment Simulation and Pollution Control, School of Environment, Tsinghua University, Beijing 100084, China*
[e] *National Local Joint Engineering Research Center for Road Engineering and Disaster Prevention and Reduction Technology in Mountainous Areas, China Merchants Chongqing Communications Technology Research and Design Institute Co., Ltd., Chongqing 400067, China*
[f] *Chongqing Culture Relics and Archaeology Research Institute, Chongqing 400013, China*

ARTICLE INFO

Article history:
Received 26 August 2023
Revised 6 December 2023
Accepted 22 December 2023
Available online 26 December 2023

Keywords:
Porphyrin-based MOFs
Single-atom Pd
Ultrathin 2D nanosheets
Hydrogen evolution
NO removal

ABSTRACT

Single-atom catalysts were widely used to treat atmospheric pollution and alleviate energy crises through photocatalysis. However, how to prevent the aggregation of single atoms during the preparation and catalytic processes remained a great challenge. Herein, a novel ultrathin two-dimensional porphyrin-based single-atom photocatalyst Ti-MOF (abbreviated as TMPd) obtained through a simple hydrothermal synthesis strategy was used for photocatalytic hydrogen evolution and NO removal, in which the single-atom Pd tightly anchored in the center of porphyrin to ensure single-atom Pd stable existence. Compared with most reported MOFs-based photocatalysts, the TMPd showed an excellent hydrogen evolution rate (1.32 mmol g^{-1} h^{-1}) and the NO removal efficiency (62%) under visible light irradiation. Aberration-corrected high-angle annular dark-field scanning transmission electron microscope (HAADF-STEM) and synchrotron-radiation-based X-ray absorption fine-structure spectroscopy (XAFS) proved that pd in TMPd existed in an isolated state, and the atomic force microscope (AFM) proved the ultrathin morphology of TMPd. DFT calculations had demonstrated that single-atom Pd could serve as the active center and more effectively achieve electron transfer, indicating that single-atom Pd played a vital role in photocatalytic hydrogen evolution. In addition, a possible photocatalytic pathway of NO removal was proposed based on ESR and *in-situ* infrared spectra, in which the catalysts anchored with single-atom Pd could produce more active substances and more effectively oxidize NO to NO_2^- or NO_3^-. The results suggested that coordinating single-atom metal species as the active site in the center of porphyrin could be a feasible strategy to obtain various ultrathin porphyrin-based single-atom photocatalysts to acquire excellent photocatalytic performance further.

With the rapid development of the human economy and social civilization, the demand for energy, especially fossil fuels, is gradually increasing, leading to growing severe problems of air pollution (NO_x, SO_x) and energy shortages, which have attracted the violent attention of the general public [1–5]. A series of "end-of-pipe" technologies have been developed to deal with the existing pollutants and significantly contribute to improving the environment [6]. However, many of these "end-of-pipe" technologies merely divert pollutants and do not completely eliminate them, which is just a treatment for symptoms rather than a cure [7]. The most fundamental approach is to control the production of contaminants at the source, *i.e.*, a "source control" strategy, thereby reducing the pressure on the subsequent treatment of pollutants [2,8]. The de-

* Corresponding authors.
E-mail addresses: zchua@nsmc.edu.cn (C. Zhang), zxf@cqjtu.edu.cn (X. Zhao), yzhectbu@163.com (Y. He).
[1] These authors contributed equally to this work.

https://doi.org/10.1016/j.cclet.2023.109455
1001-8417/

velopment and utilization of clean energy can reduce the need for fossil fuels, decrease the production of pollutants and improve energy shortages [9,10]. Therefore, to solve the problem of environmental pollution and energy shortage, we should seek a technology that could realize both "end-of-pipe treatment" and "source control" simultaneously. Photocatalysis, the use of light energy to facilitate catalytic reactions [11,12], provides a reliable pathway for treating pollutants and developing clean energy [13]. However, in the photocatalytic reaction, most of the photocatalysts have poor photocatalytic effects due to the low carrier separation and transfer efficiency [14–17]. Therefore, the search for an efficient photocatalytic material is particularly urgent.

Single-atom photocatalysts (SAPs), a multifunctional material prepared by dispersing the isolated metal atom on relevant semiconductor carriers, have recently received increasing attention because of their maximum atom utilization and excellent catalytic performance [18]. Compared with corresponding nanoclusters or nanoparticles, in addition to the well-known maximum atom-utilization efficiency and well-defined active site, the special electronic structures and unsaturated sites would endow single-atom more excellent activity and selectivity [19]. Zhang *et al.* synthesized tungsten single-atom photocatalyst by direct calcination, which can significantly promote the conversion of CH_4 into highly selective oxidation products [20]. However, the higher specific surface energy usually makes these isolated atoms easier to aggregate, especially in the synthesis process, which hinders the extensive fabrication of SAPs [21]. To our knowledge, the semiconductor carriers that the isolated atoms are anchored on are very important in hindering the individual atoms' aggregate. Therefore, it is very critical to adopt an effective semiconductor carrier that could stabilize these isolated atoms.

Metal-organic frameworks (MOFs) [22,23] is a novel type of photocatalytic materials, which are widely used in areas such as water decomposition, NO_x removal [22,24]. It is known that the organic ligands with various heteroatoms could be perfect attachment sites for individual metal atoms *via* forming the effective chemical bond, which could reduce the migration and aggregation by stabilizing these isolated atoms in the synthesis process [25,26]. The porphyrin molecule, a very famous skeleton with four pyrroles N, has been widely used as the organic ligand to fabricate the multifunctional porphyrin-based MOFs, in which four pyrrole N could coordinate with the isolated metal to further obtain confined single-atom for catalysis. Compared with bulk porphyrin-based MOFs, the confined single-atom in 2-dimensional MOFs (2D MOFs) can expose more available active sites due to the ultra-thin thickness [27,28], which is conducive to the transfer of photogenerated charge carriers and significantly inhibits the recombination efficiency of photoinduced electron-hole pairs, thus improving the photocatalytic performance [29,30].

Herein, the Pd(II) tetrakis (4-carboxyphenyl) porphyrins (PdTCPP) as organic ligands and Ti-oxo clusters as metal nodes are adopted to synthesize the ultra-thin 2D porphyrin-based MOFs for photocatalytic hydrogen evolution and NO removal, in which single-atom Pd has been anchored by the four nitrogen atoms on the pyrrole at the center of the porphyrin ring. Moreover, as the PdTCPP has a broad visible light harvesting ability and Ti-oxo clusters could serve as the famous TiO_2, the TMPd (The ligand in the synthesized sample is TCPP, abbreviated as TMH, and the ligand is PdTCPP, abbreviated as TMPd.) exhibits excellent photocatalytic performance in hydrogen evolution and NO removal. Under the irradiation of visible light, the hydrogen evolution rate can reach 1.32 mmol g^{-1} h^{-1}, and NO removal efficiency can reach 62%, which suggests the coordination of single-atom metal species as the active site in the center of porphyrin really could be a feasible strategy to obtain various 2D single-atom porphyrin-based photocatalysts to further enhance photocatalytic performance

Fig. S1 (Supporting information) showed the X-ray diffraction (XRD) patterns of TMH and TMPd, which exhibited an obvious diffraction peak near at $2\theta = 4.5°$ and could be attributed to the (002) facet [31]. At the same time, there was no characteristic diffraction peak that could be attributed to pd nanoparticles (standard card PDF #87–0645) in TMPd, indicating that Pd in TMPd had no obvious aggregation. In addition, the content of Pd in TMPd measured was 2.79% by ICP-OES. Surprisingly, the specific surface area of TMH was 331.7 m^2/g and 377.2 m^2/g for TMPd (Fig. S3 and Table S1 in Supporting information). It was probable that the coordination of Pd in the center of porphyrin made the synthesized TMPd have more microporous channels and increase the specific surface area concurrently. At the same time, the pore size distribution showed that the pore size distribution of TMH and TMPd were approximately the same. The transmission electron microscope (TEM) image of TMPd (Fig. 1a) exhibited the thin layer morphology with lateral size up to hundreds of nanometers. As displayed in the Fig. 1b, the AFM image of TMPd demonstrated that the thickness of the catalyst was less than 4 nm, and it had a relatively smooth planar structure [31]. High-resolution transmission electron microscopy (HRTEM) image (Fig. 1c) revealed that there was no periodic lattice stripe of Pd nanoparticles in TMPd, further indicating that no Pd nanoparticles were formed unambiguously, which is in line with the XRD. In addition, the elemental mapping images (Fig. 1d) demonstrate the elements of C, N, O, Ti, and Pd are evenly spread around the TMPd nanosheets. In summary, XRD, Fourier transform infrared (FT-IR) (Fig. S2 in Supporting information), Brunauer-Emmett-Teller (BET) and HRTEM analysis could in-

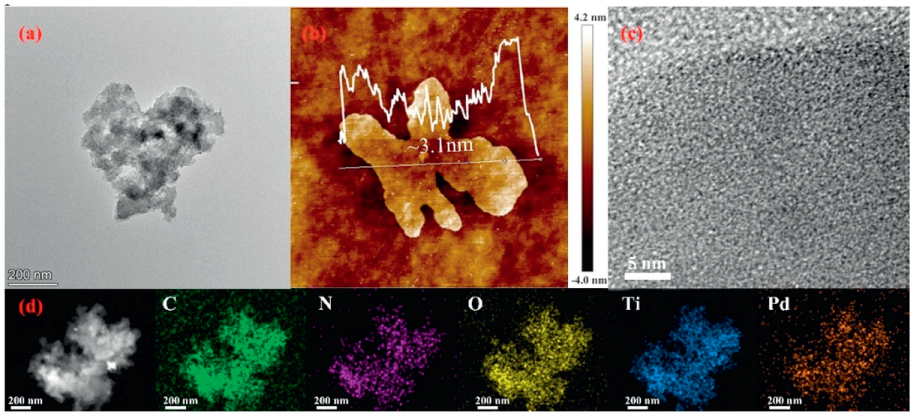

Fig. 1. (a)TEM, (b) AFM, (c) HRTEM and (d) elemental mapping images of TMPd.

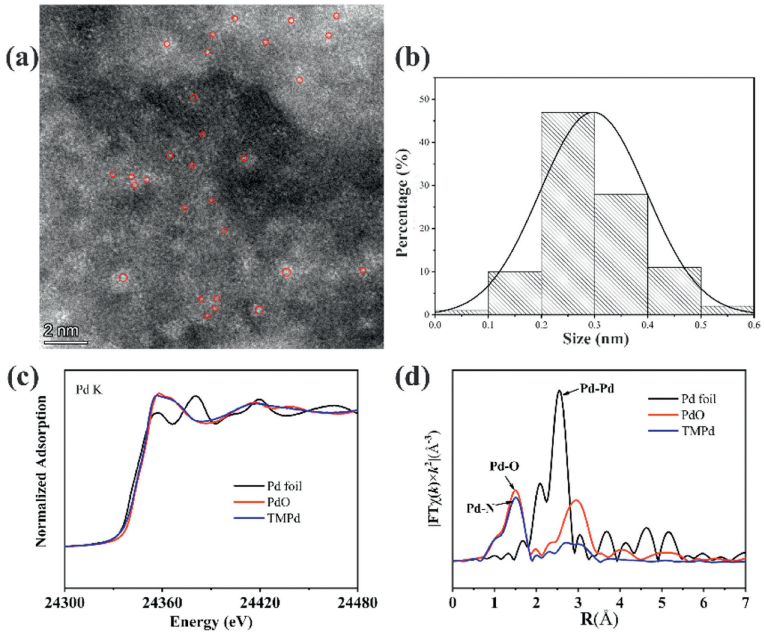

Fig. 2. Characterizations of the single-atom Pd. (a) Aberration-corrected HAADF-STEM image of the TMPd. (b) Statistical size distribution of 100 bright spots in (a). (c) The normalized Pd K-edge XANES spectra for Pd foil, PdO, and TMPd. (d) Fourier transform K-edge EXAFS spectra for Pd foil, PdO, and TMPd.

dicate that the sample TMH/TMPd had been successfully synthesized. In addition, AFM and TEM demonstrated the ultra-thin structure of TMPd.

As mentioned above in Fig. 2a, it could be clearly observed that a large number of small bright spots were distributed in the figure through an aberration-corrected high-angle annular dark-field scanning transmission electron microscope (HAADF-STEM). Meanwhile, as shown in Fig. 2b, the particle size was mainly distributed between 0.2 and 0.4 nm, which further proved that Pd existed as the isolated single atom [32]. By comparing the normalized Pd K-edge XANES spectra for the Pd element (Fig. 2c), it could be seen the Pd element in the sample existed in the oxidation state. The fitting results (Fig. S4 and Table S2 in Supporting information) and the analysis of Fourier transform extended X-ray absorption fine structure spectroscopy (EXAFS) (Fig. 2d) confirmed the main oxidation characteristics of Pd at 1.53 Å, and revealed the Pd-N coordination in the TMPd [33]. Meanwhile, it could be clearly seen from the figure that there was no obvious metal Pd-Pd bond at 2.54 Å [33], which indicated that the TMPd unambiguously contained the Pd single-atom form. The results of X-ray photoelectron spectroscopy (Fig. S5 in Supporting information) indicated that Pd in TMPd coordinates with the N atom in the porphyrin center, further proving that it was anchored at the porphyrin center in a single-atom form. It was worth noting that the optical and electrochemical properties (Fig S8 in Supporting information) of TMPd were much better than TMH, due to its ultra-thin structure and anchoring of single-atom Pd.

The photocatalytic hydrogen evolution and NO removal experiments were conducted separately in different reaction systems. The catalytic hydrogen evolution results of the materials were shown in Fig. 3a. TMH showed few photocatalytic hydrogen evolution performances, while TMPd showed a hydrogen evolution rate of up to 1.32 mmol g^{-1} h^{-1}, indicating that the complexation of single-atom Pd at the center of the porphyrin ligand could greatly enhance the photocatalytic hydrogen evolution performance. In order to investigate whether the enhanced photocatalytic hydrogen evolution performance was ascribed to the metal Pd or the complex PdTCPP, the TMH photocatalytic hydrogen evolution system was evaluated by adding the same amount of Pd ion as

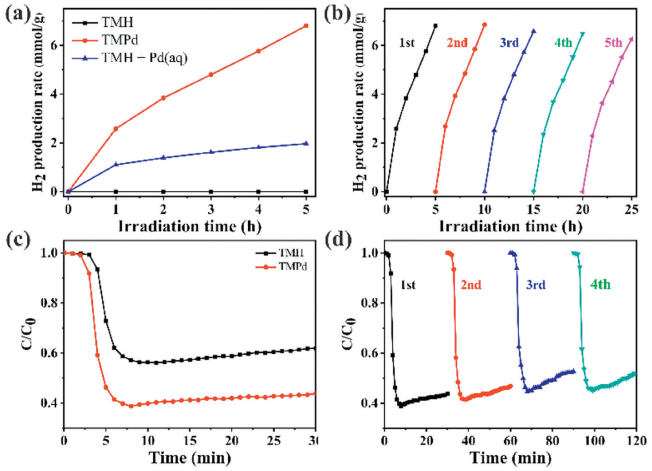

Fig. 3. (a) Photocatalytic hydrogen evolution diagram of TMH, TMPd and TMH + Pd (aq). (b) Stability tests of photocatalytic hydrogen evolution of TMPd. (c) Photocatalytic NO purification performance of TMH and TMPd. (d) Stability test of NO purification of TMPd.

the Pd content (2.79%) in TMPd under the same photocatalytic process. It was found that the photocatalytic hydrogen evolution process could be achieved at a rate of 0.39 mmol g^{-1} h^{-1}, which was only 29.5% of the TMPd evolution rate, suggesting that the higher utilization of Pd can be achieved by embedding single-atom Pd into the center of TCPP. Fig. 3b displayed the results of several consecutive photocatalytic hydrogen evolution cycles of TMPd, which demonstrated that the hydrogen evolution rate only slightly decreased after five cycles, indicating good cycling stability for further practical application. Moreover, the photocatalytic NO removal performance of TMH and TMPd was shown in Fig. 3c. The removal rate of NO for TMH was about 44%, while the removal rate of TMPd could be as high as 62%, an improvement of 18%. And the NO removal process was repeated with TMPd and the NO removal rate did not decrease much after several repetitions of the test (Fig. 3d), indicating that the TMPd had a relatively good stability in

the photocatalytic NO removal process. Surprisingly, the XPS and TEM images of TMPd after the photocatalytic experiment showed little change in the chemical state and surface morphology of TMPd, indicating its good stability (Figs. S14 and S15 in Supporting information). Meanwhile, compared with other reported literature (Tables S3 and S4 in Supporting information), TMPd also has an excellent photocatalytic hydrogen production and NO removal effect.

The electron spin resonance (ESR) tests of TMH and TMPd were shown in Fig. S9 (Supporting information). Under the no-light condition, and there was no production of both $^{\bullet}O_2^-$ and $^{\bullet}OH$ for both TMH and TMPd, while after turning on the light, two sets of signals were detected with signal intensities of approximately 1:2:2:1 and 1:1:1:1, which could correspond to radical species of $^{\bullet}OH$ and $^{\bullet}O_2^-$ respectively. It was also found that both sets of signal intensities were stronger for TMPd than for TMH, suggesting that TMPd could produce more abundance of $^{\bullet}O_2^-$ and $^{\bullet}OH$. Meanwhile, the NO removal experiments with free radical capture were shown in Fig. S10 (Supporting information), in which the NO removal efficiency for TMPd decreased after the addition of either PBQ or IPA, and the addition of *p*-benzoquinone (PBQ) could strongly inhibit the photocatalytic activity of TMPd, indicating the superoxide radical ($^{\bullet}O_2^-$) played a major role in the process of photocatalytic removal of NO.

The results of *in-situ* infrared spectra (DRIFTS) were shown in Fig. S11 (Supporting information). In Fig. S11a, the NO adsorption process for the TMH before turning on the light was represented, which mainly showed two signal peaks, located at 1341 cm^{-1} and 1418 cm^{-1}, that were attributed to the partial oxidation of NO to form nitrite [34]. At the same time, it could be found that the intensity of these two signal peaks was gradually increasing with the accumulation of adsorption time, indicating that more NO was oxidized to nitrite. In Fig. S11c, the signals at 1341 cm^{-1} and 1418 cm^{-1} were still clearly detected after the light was switched on, and the intensity increased more obviously with time, especially the signal peak at 1418 cm^{-1}, showing that the oxidation process was proceeding rapidly. The spectrum of TMPd displayed a distinct difference relative to the *in-situ* FT-IR spectrum of TMH during NO adsorption and reaction processes. Specifically, in Fig. S11b, the *in-situ* FT-IR spectrum of TMPd for NO adsorption before the light was switched on, a signal peak attributed to nitrite with a gradual increase in intensity with time was detected at 1418 cm^{-1} and two signal peaks were detected at 1016 cm^{-1} and 1069 cm^{-1} that could be attributed to monodentate nitrate and nitrite, respectively [35]. Following the visible light irradiation, a number of new signal peaks appeared in the *in-situ* FT-IR spectrogram of TMPd (Fig. S11d), including signals at 1154 cm^{-1}, 1179 cm^{-1}, and 1371 cm^{-1}, which could be classified as nitrate and nitrite [15,36]. Therefore, the ultra-thin 2D Ti-based porphyrin MOFs with single-atom Pd anchored in the center of porphyrin could enhance the ability to adsorb and oxidize NO

We further understand the potential mechanism of photocatalyst TMPd through density functional theory (DFT) calculations, as shown in Fig. 4. We study the electron transfer in TMPd by using the difference charge density distribution. In Fig. 4a, the electron aggregation area was in red, and the electron dissipation area was in blue. It can be observed that the charge redistribution mainly occurs near the single-atom Pd interface in the porphyrin center. In contrast, the charge density near the Ti-oxo cluster changes slightly, indicating that the single-atom Pd can receive photogenerated electrons from Ti-MOF. The local electrons generated near the catalytic active site are beneficial to the photocatalytic hydrogen evolution activity [37,38]. Moreover, Gibbs free energy of hydrogen adsorption (ΔG_{H^*}) is an effective physical quantity calculation of photocatalytic hydrogen evolution activity [39]. By comparing their Gibbs free energy (ΔG_{H^*}) and further investigating the effect of single atom Pd on photocatalytic hydrogen evolution activity, as shown in Fig. 4b, the ΔG_{H^*} values of TMPd and TMH are 0.198 eV and 0.32 eV, respectively. This indicates that TMPd can achieve effective proton/electron transfer and is more conducive to the release of molecular hydrogen [28]. In summary, DFT calculations can indicate that single atom Pd plays a positive role in electron transfer and H* conversion. TMPd has good photocatalytic hydrogen evolution activity, which is consistent with the experimental results.

On the basis of the above-mentioned analysis and literature research, a possible mechanism of photocatalytic hydrogen evolution and NO removal of TMPd was proposed, shown in Fig. 4c and Table S5 (Reactions S1–S10, Supporting information). Firstly, the TMPd absorbed photons under visible-light irradiation and excited to produce photogenerated electron-hole pairs (Reaction S1), which were further utilized in the photocatalytic system. In the photocatalytic hydrogen evolution reaction, the photogenerated electrons could be quickly diverted to the single-atom Pd in the porphyrin center, which in turn was passed to H_2O and completes the H_2 production process (Reaction S10) [40,41]. At the same time, the ascorbic acid (AA) would continuously consume photogenerated holes into dehydroascorbic acid (DHA) [42] to accelerate the charge carriers separation process. In the photocatalytic NO removal reaction, the active species involved in the NO oxidation process were mainly $^{\bullet}O_2^-$ and $^{\bullet}OH$. As shown in Fig. S13 (Supporting information), because the E_{CB} of the TMPd was −0.68 eV, which was more negative than $^{\bullet}O_2^-/O_2$ redox potential (−0.33 eV) [43] $^{\bullet}O_2^-$ should mainly originate from the adsorbed O_2 on the material surface reduced by photogenerated electrons. However, the E_{VB} of the TMPd was 1.19 eV, which was more negative than $OH^-/^{\bullet}OH$ redox potential (1.99 eV) [44], it could not be directly oxidized to obtain

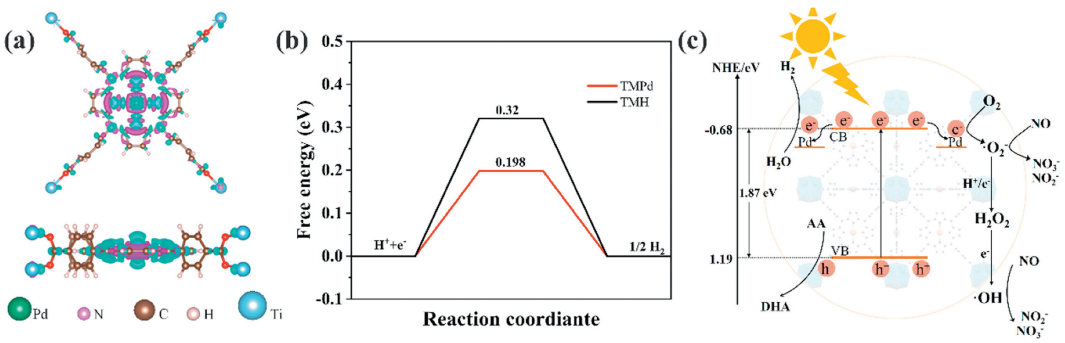

Fig. 4. (a) The differential charge density of TMPd (The equivalence surface takes the value of 0.002 eV/Å^3). (b) Hydrogen adsorption free energies of TMPd and TMH. (c) Possible mechanism for photocatalytic hydrogen evolution and NO removal of TMPd.

•OH, which needed to be obtained by Reactions S4 and S5. We detected that TMPd could generate H_2O_2 under illumination through fluorescence testing, proving that •OH was generated from H_2O_2 (Fig. S16 in Supporting information). Subsequently, the two active species ($•O_2^-$ and •OH) further converted NO to NO_2^- or NO_3^- (Reactions S6–S9).

In this paper, the ultra-thin 2D Ti-based porphyrin MOFs with single-atom Pd anchored in the center of porphyrin were prepared by a simple hydrothermal method for photocatalytic H_2 evolution and NO removal. Under illumination, the TMPd showed an excellent hydrogen evolution rate (1.32 mmol g^{-1} h^{-1}) and the NO removal efficiency (62%), which could be ascribed to the very high charge carrier separation efficiency that came from the highly efficient single-atom Pd. In addition, the ESR test displayed the main active species ($•O_2^-$ and •OH) produced under visible light irradiation, and the DRIFTS spectrum showed that TMPd was more effective than TMH in the oxidation of NO to NO_2^- or NO_3^- and can effectively suppress the production of intermediate toxic byproducts. This work inspired us that the exploitation of single-atom non-precious metal species as the active center could be a more economical avenue to obtain outstanding photocatalytic performance in the future.

Declaration of competing interest

The authors declare that they have no known competing financial interests or personal relationships that could have appeared to influence the work reported in this paper.

Acknowledgments

This work was supported by the National Natural Science Foundation of China (Nos. 22001026, 21502012), the Chongqing Science and Technology Commission (Nos. CSTB2022NSCQ-MSX1308, CSTB2023NSCQ-MSX0670), the Science and Technology Research Program of Chongqing Municipal Education Commission (No. KJZD-K202300806), Graduate Innovation Program of Chongqing Technology and Business University (No. yjscxx2023–211–41), Student Development Assistance Program of Chongqing Technology and Business University (No. 2021412237). Fund of National-local Joint Engineering Research Center for Road Engineering and Disaster Prevention and Reduction Technology in Mountainous Areas (No. SQDL-2021–01). Cultural Relics Protection Research Project of Chongqing Bureau of Cultural Relics (2022No.318). We also would like to thank the Shiyanjia Lab (www.shiyanjia.com) for the HAADF-STEM and EXAFS tests.

Supplementary materials

Supplementary material associated with this article can be found, in the online version, at doi:10.1016/j.cclet.2023.109455.

References

[1] Z. Hu, X. Zhang, Q. Yin, et al., Nano Energy 60 (2019) 775–783.
[2] C. Acar, I. Dincer, J. Clean. Prod. 218 (2019) 835–849.
[3] J. Li, R. Chen, F. Dong, et al., Nat. Commun. 13 (2022) 1098.
[4] H. Wang, K. Li, J. Li, Y. Sun, F. Dong, Environ. Sci. Technol. Lett. 8 (2021) 873–877.
[5] X. Dong, W. Cui, F. Dong, et al., Sci. Bull. 64 (2019) 669–678.
[6] Y.J. Zhang, Z.C. Han, P.Y. He, H. Chen, J. Clean. Prod. 263 (2020) 121556.
[7] A.A. Olajire, Energy 35 (2010) 2610–2628.
[8] W. Jung, M.H. Jeong, K.H. Ahn, et al., J. Hazard Mater. 391 (2020) 122223.
[9] G. Jiang, X. Liu, H. Jian, et al., Chin. Chem. Lett. 33 (2022) 3049–3052.
[10] H. Ma, Y. Liu, R. Xiong, J. Wei, Chin. Chem. Lett. 33 (2022) 1042–1046.
[11] K. Takanabe, ACS Catal. 7 (2017) 8006–8022.
[12] L. Buzzetti, G.E.M. Crisenza, P. Melchiorre, Angew. Chem. Int. Ed. 58 (2019) 3730–3747.
[13] W. Cui, J. Li, F. Dong, et al., Environ. Sci. Technol. 51 (2017) 10682–10690.
[14] W. Cui, J. Li, F. Dong, et al., J. Catal. 352 (2017) 351–360.
[15] H. Wang, Y. Sun, F. Dong, et al., Environ. Sci. Technol. 52 (2018) 1479–1487.
[16] J. Li, X. Dong, Y. Sun, W. Cen, F. Dong, Appl. Catal. B: Environ. 226 (2018) 269–277.
[17] J. Li, X. Dong, F. Dong, et al., Appl. Catal. B: Environ. 239 (2018) 187–195.
[18] B. Xia, Y. Zhang, J. Ran, M. Jaroniec, S.Z. Qiao, ACS Cent. Sci. 7 (2021) 39–54.
[19] C. Gao, J. Low, R. Long, et al., Chem. Rev. 120 (2020) 12175–12216.
[20] Y. Wang, J. Zhang, W.X. Shi, et al., Adv. Mater. 34 (2022) 1–10.
[21] J. Huang, S. Yang, S. Jiang, C. Sun, S. Song, ACS Catal. 12 (2022) 14708–14716.
[22] L. Jiao, H.L. Jiang, Chem 5 (2019) 786–804.
[23] S. Tasleem, M. Tahir, W.A. Khalifa, Int. J. Hydrog. Energy 46 (2021) 14148–14189.
[24] Y.Z. Chen, R. Zhang, L. Jiao, H.L. Jiang, Coord. Chem. Rev. 362 (2018) 1–23.
[25] K. Qi, M. Chhowalla, D. Voiry, Mater. Today 40 (2020) 173–192.
[26] B. Lu, Q. Liu, S. Chen, ACS Catal. 10 (2020) 7584–7618.
[27] Y. Zhou, L. Zheng, D. Yang, et al., Small Methods 5 (2021) 1–8.
[28] Q. Zuo, T. Liu, C. Chen, et al., Angew. Chem. Int. Ed. 58 (2019) 10198–10203.
[29] J. Zhang, Y. Wang, H. Wang, D. Zhong, T. Lu, Chin. Chem. Lett. 33 (2022) 2065–2068.
[30] W. Zhang, Y. Wang, Y. Wang, Y. Liang, F. Dong, Chin. Chem. Lett. 33 (2022) 1259–1262.
[31] X. Wang, J. Ye, D. Wang, et al., Nano Energy 62 (2019) 250–258.
[32] C. Chu, D. Huang, S. Gupta, et al., Nat. Commun. 12 (2021) 1–7.
[33] E. Zhao, M. Li, B. Xu, et al., Angew. Chem. Int. Ed. 134 (2022) e202207410.
[34] H. Feng, H. Li, X. Liu, et al., Chem. Eng. J. 428 (2022) 1–10.
[35] J. Cao, J. Zhang, X. Dong, et al., Appl. Catal. B: Environ. 249 (2019) 266–274.
[36] J. Liao, K. Li, H. Ma, et al., Chin. Chem. Lett. 31 (2020) 2737–2741.
[37] T. Lv, B. Xiao, F. Xia, et al., Chem. Eng. J. 450 (2022) 137873.
[38] Y. Zhang, J. Zhao, H. Wang, et al., Nat. Commun. 13 (2022) 58.
[39] A. Shan, X. Teng, Y. Zhang, et al., Nano Energy 94 (2022) 106913.
[40] Q. Zeng, S. Chang, M. Wang, et al., Chin. Chem. Lett. 32 (2021) 2212–2216.
[41] Q. Zhang, Y. Xiao, L. Yang, et al., Chin. Chem. Lett. 34 (2023) 107628.
[42] J. Kosco, S. Gonzalez-Carrero, C.T. Howells, et al., Nat. Energy 7 (2022) 340–351.
[43] Y. He, Y. Tan, M. Song, et al., J. Hazard. Mater. 430 (2022) 128468.
[44] F. Chang, X. Wang, S. Zhao, X. Zhang, X. Hu, Sep. Purif. Technol. 287 (2022) 120532.